COMPREHENSIVE STUDY OF OPTICAL, PHYSICAL, CHEMICAL, AND RADIATIVE PROPERTIES OF TOTAL COLUMNAR ATMOSPHERIC AEROSOLS OVER CHINA

An Overview of Sun–Sky Radiometer Observation Network (SONET) Measurements

Z. Q. Li, H. Xu, K. T. Li, D. H. Li, Y. S. Xie, L. Li, Y. Zhang, X. F. Gu, W. Zhao, Q. J. Tian, R. R. Deng, X. L. Su, B. Huang, Y. L. Qiao, W. Y. Cui, Y. Hu, C. L. Gong, Y. Q. Wang, X. F. Wang, J. P. Wang, W. B. Du, Z. Q. Pan, Z. Z. Li, and D. Bu

SONET provides the first comprehensive climatology of optical, physical, chemical composition, and radiative characteristics of atmospheric columnar aerosols over China based on long-term ground-based remote sensing measurements.

Aerosol is an important component of the planetary atmosphere and plays a key role in Earth's energy balance and global climate change. With complex composition, aerosol also has large temporal and spatial variations, making itself the biggest uncertainty source in global climate change assessment (IPCC 2013). On one hand, aerosol changes the radiation balance of the Earth–atmosphere system by scattering and absorbing sunlight. On the other hand, aerosol acts as cloud condensation nuclei, interacting with clouds and affecting cloud radiative properties. Moreover, absorptive aerosols make the aerosol–cloud–radiation interaction more complicated and yield inhibition or amplification of precipitation (Rosenfeld et al. 2001). In addition, aerosol has an important impact on air quality. In many developing countries, particulate matter (mainly fine aerosol) is the most important air pollutant. The high-concentration emissions due to anthropogenic activities, having caused a significant increase of haze events, are remarkably affecting public health and traffic safety.

China is one of the most polluted regions in the world with high aerosol loading, following measurements of Chinese Sun Hazemeter Network (CSHNET; Xin et al. 2007) and China Aerosol Remote Sensing Network (CARSNET; Che et al. 2009). Complex aerosol components resulting from industrial activities, traffic, biomass burning, and natural sources exist simultaneously over the country. Although the international Aerosol Robotic Network (AERONET) and Sky Radiometer Network (SKYNET; Nakajima et al. 2007) have taken observations in China, supporting many studies on aerosol properties (e.g.,

Kim et al. 2004; Li et al. 2007; Eck et al. 2010), the observation sites are still very rare and distributed unevenly (e.g., mainly around the Beijing area) over this vast region. Moreover, many China local researchers, usually encountering difficulties on operational measurement, maintenance, calibration, inversion, and quality control, are still very limited in acquiring high-quality and comprehensive scientific data. Therefore, there is an important lack of climatological knowledge on the total columnar atmospheric aerosols over China, especially the coincident optical, physical, chemical, and radiative properties.

The Sun–Sky Radiometer Observation Network (SONET; www.sonet.ac.cn) is a ground-based Cimel radiometer network with the extension of multiwavelength polarization measurement capability to provide long-term columnar atmospheric aerosol properties over China. In this paper, an overview of SONET infrastructure and data products is briefly introduced and then a climatology study is presented, focusing on aerosol optical, physical, chemical, and radiative properties obtained from 16 long-term SONET sites over China.

INFRASTRUCTURE. The multiwavelength polarized sun–sky radiometer CE318-DP manufactured by Cimel Electronique in France is employed by SONET. The CE318-DP is an automatic instrument for long-term continuous observation in the field. The CE318-DP owns radiance and polarization measurements with nine wavelengths (see Table 1) for aerosol and water vapor observations.

The 16 SONET automatic sites (Fig. 1) are located in typical regions of China, including urban, rural, desert, coastal, basin, mountain, and plateau areas. The sites are also routinely maintained by site managers following AERONET instrument check suggestions—for example, examining the battery voltage, verifying the instrument horizontal mounting status, and cleaning the contaminated collimator. For each site, instrument calibration is carried out once a year to ensure the data quality. Table 2 presents the basic information of the 16 sites classified by four typical climate zones.

DATA PRODUCT. *Products and data levels.* More than 20 kinds of aerosol parameter products (Table 3) can be obtained from SONET measurements, which are classified into four major categories (optical, physical, chemical, and radiative properties). Most of these data products are described in the AERONET documentations (e.g., Holben et al. 1998; Dubovik and King 2000; Dubovik et al. 2006). Except for standard AERONET products, the chemical component fractions of columnar aerosol, the additional products of SONET, are derived on the basis of the retrieved optical and physical parameters following recent studies (e.g., Schuster et al. 2005; Ganguly et al.

Table 1. Wavelengths, bandwidths, and polarization of the sun–sky radiometer CE318-DP. FWHM = full width at half maximum.

Bands (nm)	340	380	440	500	675	870	936	1,020	1,640
FWHM (nm)	2	4	10	10	10	10	10	10	25
Polarization (yes/no)	Yes	Yes	Yes	Yes	Yes	Yes	No	Yes	Yes

AFFILIATIONS: Z. Q. Li, H. Xu, K. T. Li, D. H. Li, Y. S. Xie, L. Li, Y. Zhang and X. F. Gu—State Environmental Protection Key Laboratory of Satellite Remote Sensing, Institute of Remote Sensing and Digital Earth, Chinese Academy of Sciences, Beijing, China; W. Zhao—National Satellite Ocean Application Service, Beijing, China; Q. J. Tian—Nanjing University, Nanjing, China; R. R. Deng—Sun Yat-sen University, Guangzhou, China; X. L. Su—Institute of Earth Environment, Chinese Academy of Sciences, Xi'an, China; B. Huang—Zhejiang Provincial Zhoushan Marine Ecological Environmental Monitoring Station, Zhoushan, China; Y. L. Qiao and W. Y. Cui—Anhui Institute of Optics and Fine Mechanics, Chinese Academy of Sciences, Hefei, China; Y. Hu and C. L. Gong—Shanghai Institute of Technical Physics, Chinese Academy of Sciences, Shanghai, China; Y. Q. Wang—Chengdu University of Information Technology, Chengdu, China; X. F. Wang—Heilongjiang University, Harbin, China; J. P. Wang and W. B. Du—Kashi Data Receiving Station, Institute of Remote Sensing and Digital Earth, Chinese Academy of Sciences, Beijing, China; Z. Q. Pan and Z. Z. Li—China Centre for Resources Satellite Data and Application, Beijing, China; D. Bu—Tibet University, Lhasa, China

CORRESPONDING AUTHORS: Zhengqiang Li, lizq@radi.ac.cn; Hua Xu, xuhua@radi.ac.cn

The abstract for this article can be found in this issue, following the table of contents.

DOI:10.1175/BAMS-D-17-0133.1

In final form 5 November 2017

2009; Wang et al. 2013). Five aerosol components—black carbon (BC), brown carbon (BrC), coarse-mode component (CM), fine-mode scattering component (FS), and aerosol water (AW)—are estimated from SONET measurements (Li et al. 2013). The CM component can be further inferred as sea salt (SS) at coastal and island sites or mineral dust (DU) at inland sites. It is also noted that there are new polarized parameters (i.e., $-F_{12}$) derived from SONET's additional multiwavelength polarization measurements, which might be useful for further analysis, for example, identification of aerosol shape (Huang et al. 2015).

The aerosol optical depth (AOD)-related products [including AOD, Ångström exponent (AE), and fine-mode fraction (FMF)] are graded into three levels (1.0, 1.5, and 2.0). These level definitions follow the AERONET data level protocols (version 2). Briefly, level 1.0 refers to raw data calculated from direct-sun measurements and AOD calibration coefficients, with all necessary instrumental corrections and extinction modifications applied. Level 1.5 is based on level 1.0 but cloud screened by automatic procedures. Level 2.0 has the additional application of pre- and postcalibration coefficients and expert checking. Inversion products [from single-scattering albedo (SSA) to nonspherical percent (NS%) in Table 3] are graded into two levels (1.5 and 2.0), following the AERONET criteria (Holben

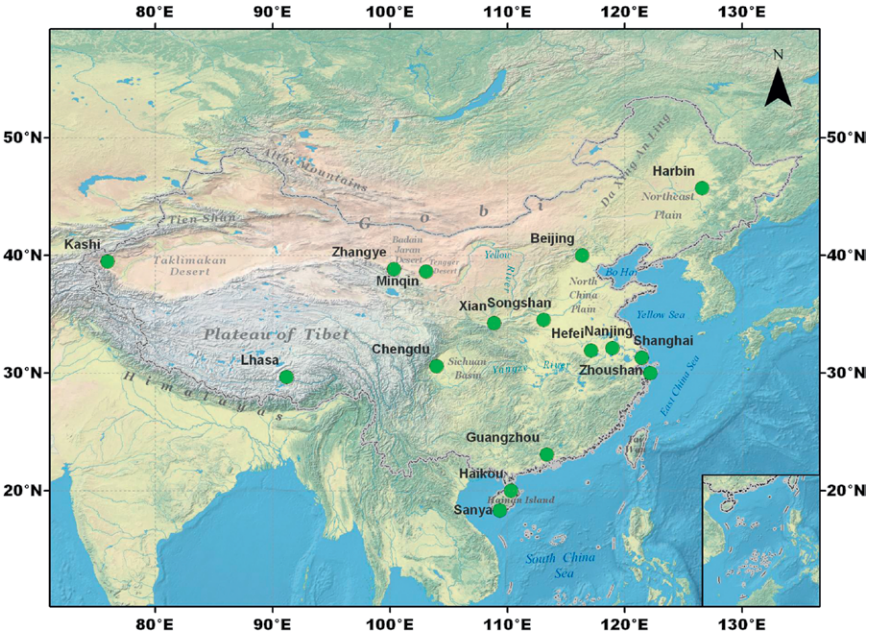

Fig. 1. Map of 16 long-term SONET sites.

Table 2. Basic information on the 16 SONET sites. Climate classification refers to Peel et al. (2007).

Climate	Site	Location	Alt (m)	Start time	Aerosol characteristics
Tropical	Sanya	18.3°N, 109.4°E	29	Aug 2014	Maritime + urban
	Haikou	20.0°N, 110.3°E	22	Mar 2014	Maritime + urban
Temperate	Guangzhou	23.1°N, 113.4°E	28	Nov 2011	Maritime + urban/PRD region
	Zhoushan	29.9°N, 122.1°E	29	Jan 2012	Maritime + urban
	Shanghai	31.3°N, 121.5°E	84	Mar 2013	Maritime + urban/YRD region
	Hefei	31.9°N, 117.2°E	36	Jan 2013	Urban/YRD region
	Nanjing	32.1°N, 119.0°E	52	Jan 2013	Urban/YRD region
	Chengdu	40.6°N, 104.0°E	510	May 2013	Urban (basin)
	Songshan	34.5°N, 113.1°E	475	Nov 2013	Urban + dust
	Xi'an	34.2°N, 108.9°E	389	May 2012	Urban + dust
Continental	Beijing	40.0°N, 116.3°E	59	Mar 2010	Urban/Beijing–Tianjin–Hebei region
	Harbin	45.7°N, 126.6°E	223	Dec 2013	Urban
Dry	Minqin	38.8°N, 100.3°E	1,589	Feb 2012	Dust
	Zhangye	38.6°N, 103.0°E	1,364	Jul 2012	Dust
	Kashi	39.5°N, 75.9°E	1,320	Jun 2013	Dust
	Lhasa	29.6°N, 91.2°E	3,678	Sep 2013	Background

et al. 2006). The qualities of chemical components and radiative parameters depend on the data levels of optical and physical data products.

Measurement calibration. To ensure the data quality, SONET established a routine calibration scheme, consisting of laboratory and field calibration approaches. AOD-related measurements are calibrated every year in the field (Ling Mountain site, ~1,600 m MSL), via intercomparison with a master instrument. The master instrument is regularly calibrated at AERONET/Photométrie pour le Traitement Opérationnel de Normalisation Satellitaire (PHOTONS) Izaña Observatory by Langley plot approach with high precision [visible/near-infrared (VIS/NIR) bands: ~0.25%–0.5%, ultraviolet (UV) bands: ~0.5%–2%; Holben et al. 1998].

For the calibration of sky radiance measurements, the SONET approach differs from that of AERONET (i.e., absolute integrating sphere method). Because of difficulties in regular maintenance of high-precision absolute calibration of the integrating sphere, the sky radiance is calibrated by using a vicarious/transfer calibration method (Li et al. 2008). The resulting radiance uncertainty is estimated to be about 3%–5%.

For sky polarization calibration, a laboratory polarization box (PolBox) is used to generate reference light with a specific degree of linear polarization (DoLP). The polarization calibration coefficient is obtained by comparing CE318-DP measurements with PolBox reference values (Li et al. 2018).

Data quality assessment. The accuracies of SONET products are assessed based on a joint SONET–AERONET dataset during the Distributed Regional Aerosol Gridded Observational Network (DRAGON)–Korea–United States Air Quality Study (KORUS-AQ) 2016 campaign (Holben et al. 2018). The observation and calibration are conducted by SONET at six sites (Harbin, Nanjing, Hefei, Shanghai, Zhoushan, and Xingtai), but AOD and inversions are produced in parallel by SONET and AERONET, respectively. Therefore, the differences of two network products can reflect the performance of SONET.

As for AOD comparison (Table 4), it can be seen that the record number of SONET level 1.0 AODs is slightly larger than AERONET, but that of SONET

Table 3. SONET aerosol products, definitions, and units.

Products	Description	Unit
AOD (λ)	Aerosol optical depth (340, 380, 440, 500, 675, 870, 1,020, and 1,640 nm)	—
AE	Ångström exponent (440–870 nm)	—
FMF	Fine-mode fraction of aerosol optical depth (500 nm)	—
SSA (λ)	Single-scattering albedo (440, 675, 870, and 1,020 nm)	—
F_{11} (λ)	Scattering phase function (440, 675, 870, and 1,020 nm)	—
$-F_{12}$ (λ)	Polarization phase function (440, 675, 870, and 1,020 nm)	—
g (λ)	Asymmetry factor (440, 675, 870, and 1,020 nm)	—
S (λ)	Lidar ratio (440, 675, 870, and 1,020 nm)	—
$dV/d\ln r$	VPSD with 22 bins for radius from 0.05 to 15.0 μm	$\mu m^3\ \mu m^{-2}$
n (λ)	Refractive index (real part) (440, 675, 870, and 1,020 nm)	—
k (λ)	Refractive index (imaginary part) (440, 675, 870, and 1,020 nm)	—
r_{eff}	Effective radius (total, fine, and coarse modes)	μm
V	Volume concentration (total, fine, and coarse modes)	$\mu m^3\ \mu m^{-2}$
NS (%)	Percentage of nonspherical particles	—
RF	Shortwave aerosol radiative forcing (0.3–2.8 μm) at TOA or BOA	W m^{-2}
RFE	Shortwave aerosol radiative forcing efficiency [i.e., RF normalized by AOD (550 nm)]	W m^{-2}
AW (%)	Percentage of mass concentration of water uptake of aerosols	—
FS (%)	Percentage of mass concentration of fine-mode scattering components (e.g., sulfate, nitrate and light non-absorbing organic matters)	—
CM (%)	Percentage of mass concentration of coarse-mode components (dust or sea salt)	—
BrC (%)	Percentage of mass concentration of brown carbon components	—
BC (%)	Percentage of mass concentration of black carbon components	—

level 1.5 AODs is smaller than AERONET. The common record ratios of AOD products are above 95%, indicating quite comparable scientific data acquisition capability of both SONET and AERONET.

In Table 5, it is shown that the average AOD difference (0.002 ± 0.001) between SONET and AERONET is much smaller than the AERONET AOD uncertainty. The AERONET AOD is the most accurate measurement of the total columnar aerosol optical properties, whose accuracy relies on calibration, algorithm, and instrument performance. According to Holben et al. (1998), by transferring high mountain calibration (e.g., at Mauna Loa Observatory in Hawaii) to field CE318 instruments, the absolute AOD uncertainty can be less than about 0.01–0.02 (slightly larger at UV and NIR bands). Here, the AOD difference (0.002 ± 0.001) reflects mainly the processing code (algorithm) difference between two networks, while the calibration difference is minimized in SONET by employing master instruments directly calibrated by AERONET/PHOTONS. The average difference on SSA is slightly large, while differences of all other parameters are less than or close to the AERONET nominal uncertainties. This suggests that not only are the two networks comparable, but the accuracies of both networks are also quite high.

AEROSOL CLIMATOLOGY OVER CHINA.

From Fig. 2 (the multiyear AOD time series at SONET sites), it can be seen that aerosol loadings over China are highly variable in spatial and temporal distribution. Moreover, aerosol properties are complex, so comprehensive parameters, describing aerosol from different aspects, are needed to provide a complete description of aerosols. In this paper, we select the most representative SONET products (see Tables 6 and 7) to analyze China aerosol characteristics, including 1) optical parameters (AOD, AE, FMF, and SSA), 2) physical parameters [volume particle size distribution (VPSD)], 3) chemical composition parameters [BC%, BrC%, CM%, FS%, AW%, and total mass concentration (TMC)], and 4) radiative parameters [radiative forcing (RF) and radiative forcing efficiency (RFE) at top of atmosphere (TOA) and bottom of atmosphere (BOA), respectively]. Moreover, we utilize level 2.0 products in all cases, except that we employed level 1.5 inversion data instead of level 2.0 at the Lhasa site, where very low aerosol loading prohibits gathering enough inversion records even in the month scale. As a compensation, however, we applied all remaining level 2.0 criteria (only expect for AOD > 0.4 threshold) for the Lhasa site to ensure the inversion data quality.

Optical properties. Spatial variation. In a map of China, the Heihe–Tengchong Line (Hu 1935), a nearly 45° diagonal straight line from northeast to southwest China, separates the country into two

Table 4. Statistics on record numbers of SONET and AERONET AOD data at six sites (May and Jun 2016).

Data level	AERONET	SONET	Common counts	Common record ratio
Level 1.0	6,199	6,245	6,013	96.3%
Level 1.5	2,805	2,769	2,679	95.5%

Table 5. Comparison of SONET and AERONET aerosol products over six sites (May and Jun 2016).

Parameters	Diff (avg and std dev) from AERONET	AERONET uncertainty
AOD	0.002 ± 0.001	0.01–0.02[a]
AE	0.01 ± 0.02	—
FMF	0.002 ± 0.03	0.1[b]
SSA	0.02 ± 0.04	0.03[c]
n	0.007 ± 0.04	0.04[c]
k	18% ± 46%	40%[c]
$dV/d\ln r$	1.5% ± 26% ($0.1 < r < 7$ μm) 18% ± 85% ($r < 0.1$ μm and $r > 7$ μm)	25%[c] ($0.1 < r < 7$ μm) 25%–100% ($r < 0.1$ μm and $r > 7$ μm)

[a] Holben et al. (1998).

[b] O'Neill et al. (2001).

[c] Dubovik et al. (2000).

distinct geographical areas, not only in population-density aspect but also in the economic and ecological meanings. According to multiyear SONET observation products, the spatial distribution of aerosol optical properties also roughly follows this pattern.

As shown in Figs. 3a–c, low aerosol loading appears in the western region of China, where it is less populated and mainly affected by natural dust. At Minqin and Zhangye, the multiyear average AODs (500 nm) are the lowest (<0.3). Meanwhile, their average AEs (440–870 nm) and FMFs (500 nm) are also low (less than 0.7 and 0.5, respectively). The Kashi site, which is also in the western region but close to the Taklimakan Desert, is often affected by dust, where AOD is obviously higher (0.56), while AE and FMF are the lowest among all sites. The Lhasa site (3,600 m MSL) in the Tibetan Plateau is the cleanest site (AOD < 0.1) with FMF about 0.55. In contrast, AOD in the central and eastern regions, especially in densely populated eastern China, is generally higher than western areas. The AE and FMF are mostly larger than 1.1 and 0.7, respectively, which implies dominant fine particles. The Chengdu site, located in the populated Sichuan basin, shows the largest AOD (0.93) and FMF (0.81) among all sites. In the northeastern plain, AOD at Harbin is relatively low (0.38), with a higher proportion of fine particles (FMF close to 0.8). In tropical areas, AOD at Sanya is moderate (0.42) but FMF is as low as only 0.66, indicating the probable influence of sea salt.

SSA represents light absorption fraction among total light extinction of aerosols. The multiyear average SSA (675 nm) of SONET sites is between 0.84 and 0.95 (see Fig. 3d). The strongest absorption (low SSA) presents at Beijing and Harbin (~0.91), indicating a high content of absorbing aerosols (e.g., BrC and BC). Lhasa shows also low SSA, but as mentioned above, this value is in doubt (level 1.5) because it suffers from much larger uncertainty. The weakest aerosol absorption (SSA ~ 0.95) appears at coastal Haikou and Zhoushan (affected by maritime aerosols) and northwestern Minqin and Zhangye (affected by dust aerosols). The two former sites are similar to Hawaii's Lanai site (SSA ~ 0.97), and the two latter sites are comparable to the Solar Village site in Saudi Arabia (SSA ~ 0.96; Dubovik et al. 2002). Overall, SSA in China is about 0.93 on average, while slightly higher at coastal (e.g., Zhoushan and Haikou) and dust sites (e.g., Zhangye and Minqin) than continental sites (e.g., Beijing, Xi'an, Chengdu, and Harbin).

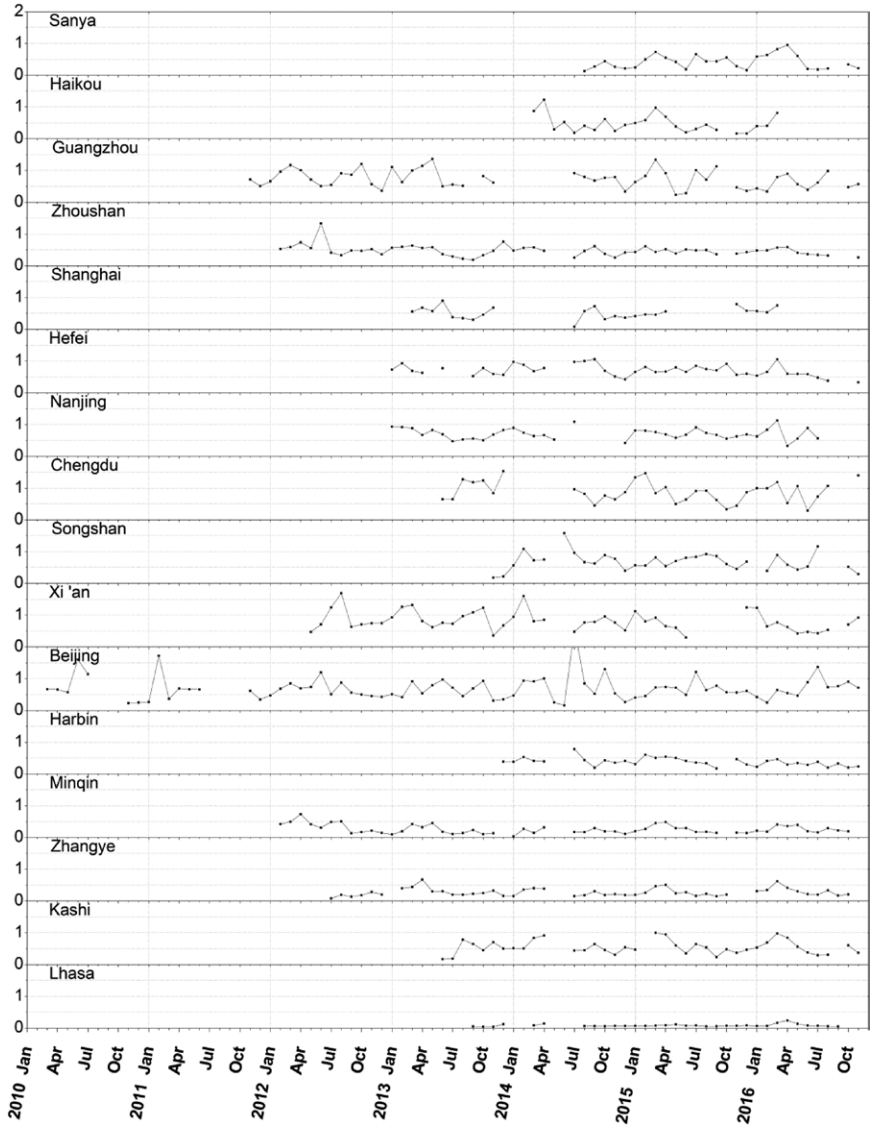

Fig. 2. Multiyear monthly average AOD (500 nm) at SONET sites.

Seasonal variations. The multiyear seasonal average AOD (500 nm) and monthly average AE (440–870 nm) are shown in Fig. 4. These results reveal several seasonal variation patterns:

1) *Western and arid regions*: Both seasonal trends of AOD and AE at Minqin and Zhangye (about 250-km distance apart) are very similar. Because of frequent dust invasion in spring, AOD is the highest from March to May, and AE correspondingly reaches the lowest value. At Kashi, dust influence seems to be much stronger (e.g., AOD in spring is almost twice as much as those at Minqin and Zhangye). At Lhasa, AOD is very low but increases slightly in spring.
2) *Tropical region*: Both AOD and AE in spring are higher than other seasons at Sanya and Haikou. In summer, AOD drops to a low level when AE decreases, which suggests the prevalence of maritime aerosols during June–August.
3) *Central and eastern regions*: AOD in the Yangtze River delta (YRD) region (Hefei, Nanjing, Shanghai, and Zhoushan) shows a similar seasonal pattern, and the nearer the ocean is, the smaller the AOD is. At Hefei, Nanjing, and Shanghai, AE also illustrates a similar seasonal pattern, that is, relatively large from July to September. In the Pearl River delta (PRD) region (Guangzhou site), AOD is higher in spring and autumn, and AE is slightly low in summer. At Chengdu, AOD is notably high in all seasons, especially in winter. AE is also high (up to 1.48) all the year, especially in summer. At Beijing and Songshan, the highest AOD appears in summer while the lowest is in winter. At Xi'an, AE is relatively low in spring, indicating dust impacts. At Harbin, AOD is less than 0.5 in all seasons, and AE keeps stable and very high

Table 6. Multiyear average aerosol optical and radiative properties at SONET sites.

Sites	AOD (500 nm)	AE (440–870 nm)	FMF (500 nm)	SSA (440 nm)	SSA (675 nm)	SSA (870 nm)	SSA (1,020 nm)	RF (TOA)	RFE (TOA)	RF (BOA)	RFE (BOA)
Sanya	0.42 ± 0.20	1.10 ± 0.23	0.66 ± 0.16	0.94 ± 0.02	0.93 ± 0.03	0.91 ± 0.04	0.89 ± 0.05	−10.76	−20.51	−30.64	−56.15
Haikou	0.47 ± 0.24	1.25 ± 0.22	0.76 ± 0.14	0.96 ± 0.03	0.95 ± 0.03	0.94 ± 0.04	0.93 ± 0.05	−14.74	−26.65	−30.25	−52.73
Guangzhou	0.72 ± 0.20	1.26 ± 0.08	0.81 ± 0.11	0.94 ± 0.03	0.94 ± 0.03	0.92 ± 0.04	0.90 ± 0.05	−14.87	−22.67	−35.19	−53.91
Zhoushan	0.48 ± 0.09	1.19 ± 0.05	0.74 ± 0.15	0.95 ± 0.02	0.95 ± 0.02	0.94 ± 0.03	0.93 ± 0.04	−16.41	−29.28	−29.80	−53.66
Shanghai	0.53 ± 0.13	1.26 ± 0.10	0.76 ± 0.14	0.92 ± 0.05	0.92 ± 0.05	0.91 ± 0.05	0.89 ± 0.06	−10.26	−18.62	−43.39	−69.31
Hefei	0.69 ± 0.10	1.20 ± 0.12	0.78 ± 0.14	0.92 ± 0.03	0.93 ± 0.03	0.92 ± 0.04	0.90 ± 0.05	−16.05	−26.03	−38.00	−62.99
Nanjing	0.71 ± 0.10	1.21 ± 0.11	0.74 ± 0.15	0.91 ± 0.03	0.92 ± 0.03	0.91 ± 0.03	0.89 ± 0.04	−13.14	−22.35	−36.81	−59.56
Chengdu	0.93 ± 0.20	1.21 ± 0.11	0.81 ± 0.13	0.93 ± 0.04	0.94 ± 0.03	0.94 ± 0.03	0.92 ± 0.04	−17.26	−22.64	−33.19	−43.48
Songshan	0.69 ± 0.14	1.12 ± 0.14	0.73 ± 0.16	0.93 ± 0.03	0.94 ± 0.03	0.93 ± 0.04	0.92 ± 0.04	−16.11	−24.56	−29.76	−45.96
Xi'an	0.81 ± 0.17	1.03 ± 0.16	0.67 ± 0.17	0.90 ± 0.04	0.93 ± 0.03	0.93 ± 0.03	0.92 ± 0.04	−13.84	−19.03	−33.71	−47.60
Beijing	0.68 ± 0.22	1.06 ± 0.10	0.67 ± 0.17	0.90 ± 0.04	0.91 ± 0.04	0.90 ± 0.04	0.88 ± 0.05	−17.99	−23.49	−45.95	−62.35
Harbin	0.38 ± 0.08	1.34 ± 0.09	0.79 ± 0.14	0.92 ± 0.04	0.91 ± 0.04	0.90 ± 0.05	0.88 ± 0.06	−14.43	−26.72	−31.10	−59.33
Minqin	0.26 ± 0.11	0.70 ± 0.27	0.48 ± 0.19	0.94 ± 0.04	0.95 ± 0.04	0.95 ± 0.04	0.95 ± 0.05	−9.86	−17.66	−11.03	−19.80
Zhangye	0.28 ± 0.11	0.66 ± 0.20	0.43 ± 0.14	0.94 ± 0.03	0.95 ± 0.04	0.95 ± 0.04	0.95 ± 0.04	−11.92	−22.31	−13.09	−24.39
Kashi	0.56 ± 0.18	0.54 ± 0.27	0.40 ± 0.14	0.92 ± 0.03	0.94 ± 0.03	0.95 ± 0.03	0.95 ± 0.04	−15.72	−20.84	−17.93	−24.02
Lhasa	0.09 ± 0.03	0.73 ± 0.08	0.55 ± 0.13	0.84 ± 0.04	0.84 ± 0.04	0.82 ± 0.05	0.80 ± 0.05	−1.22	−17.19	−1.39	−18.67

Table 7. Multiyear average aerosol physical and chemical composition properties at SONET sites. VPSD parameters (r_f, r_c, σ_f, σ_c, V_f, and V_c) are median radius, geometric standard deviation, and volume concentration of fine (f) and coarse (c) modes, respectively.

Sites	r_f (μm)	r_c (μm)	σ_f (μm)	σ_c (μm)	V_f ($\mu m^3\ \mu m^{-2}$)	V_c ($\mu m^3\ \mu m^{-2}$)	BC (mg m^{-2})	BrC (mg m^{-2})	CM (DU or SS) (mg m^{-2})	FS (mg m^{-2})	AW (mg m^{-2})
Sanya	0.18 ± 0.03	2.84 ± 0.60	0.48 ± 0.07	0.67 ± 0.07	0.07 ± 0.06	0.05 ± 0.04	2.07	8.23	59.69	52.73	91.38
Haikou	0.18 ± 0.03	2.91 ± 0.55	0.49 ± 0.08	0.65 ± 0.08	0.09 ± 0.06	0.06 ± 0.06	1.60	8.81	74.50	65.59	103.30
Guangzhou	0.21 ± 0.05	3.13 ± 0.55	0.55 ± 0.07	0.61 ± 0.06	0.13 ± 0.09	0.07 ± 0.11	3.53	12.58	80.15	80.50	123.37
Zhoushan	0.18 ± 0.05	2.77 ± 0.50	0.53 ± 0.08	0.62 ± 0.05	0.08 ± 0.06	0.08 ± 0.08	1.69	10.43	127.45	71.31	89.00
Shanghai	0.18 ± 0.05	2.89 ± 0.52	0.53 ± 0.09	0.63 ± 0.06	0.10 ± 0.07	0.09 ± 0.13	7.04	24.16	118.97	64.91	88.09
Hefei	0.19 ± 0.06	2.88 ± 0.47	0.52 ± 0.07	0.63 ± 0.05	0.11 ± 0.07	0.10 ± 0.08	3.55	3.58	244.92	39.46	94.99
Nanjing	0.18 ± 0.05	2.92 ± 0.44	0.53 ± 0.09	0.63 ± 0.05	0.11 ± 0.07	0.09 ± 0.06	4.84	5.46	247.81	34.58	97.44
Chengdu	0.20 ± 0.05	2.87 ± 0.52	0.55 ± 0.07	0.62 ± 0.06	0.15 ± 0.09	0.10 ± 0.06	3.30	6.09	245.96	39.59	113.73
Songshan	0.18 ± 0.06	2.84 ± 0.44	0.51 ± 0.07	0.63 ± 0.05	0.10 ± 0.08	0.11 ± 0.10	3.14	3.46	270.31	43.21	106.26
Xi'an	0.17 ± 0.06	2.77 ± 0.46	0.53 ± 0.08	0.63 ± 0.06	0.12 ± 0.10	0.19 ± 0.19	4.11	11.61	432.73	56.59	112.16
Beijing	0.16 ± 0.04	3.02 ± 0.42	0.50 ± 0.07	0.64 ± 0.06	0.08 ± 0.09	0.12 ± 0.13	5.27	8.02	388.98	63.51	103.65
Harbin	0.15 ± 0.04	3.30 ± 0.42	0.51 ± 0.08	0.65 ± 0.06	0.07 ± 0.06	0.05 ± 0.09	3.90	2.49	205.59	58.62	74.87
Minqin	0.15 ± 0.03	2.49 ± 0.41	0.51 ± 0.07	0.65 ± 0.06	0.03 ± 0.02	0.11 ± 0.15	0.95	0.02	416.94	139.36	92.20
Zhangye	0.14 ± 0.02	2.52 ± 0.42	0.51 ± 0.06	0.65 ± 0.05	0.02 ± 0.01	0.12 ± 0.15	0.95	0.01	498.44	212.75	69.43
Kashi	0.15 ± 0.03	2.49 ± 0.52	0.56 ± 0.09	0.62 ± 0.08	0.04 ± 0.03	0.30 ± 0.37	1.33	0.76	822.80	329.80	111.37
Lhasa	0.14 ± 0.02	3.15 ± 0.37	0.51 ± 0.06	0.66 ± 0.05	0.01 ± 0.02	0.04 ± 0.09	1.81	0.24	94.3	7.38	3.99

throughout the year, suggesting less influence of coarse aerosols.

Figure 5 shows the multiyear seasonal average spectral SSA and monthly average FMF.

1) *Western and arid regions:* At Kashi, dust events frequently occur, and thus the spectral SSA presents an obvious dust feature (i.e., SSA grows with the increase of wavelengths from 440 to 675 nm). However, this increment is reduced in winter. Meanwhile, FMF is the lowest in spring, and then jumps highly in December, indicating enhanced anthropogenic influences. At Minqin, there are similar dust patterns but the SSA feature is relatively weak, while those at Zhangye (especially the SSA feature) are significantly disturbed.
2) *Tropical region:* At Sanya and Haikou, SSA is lower in spring and winter, which might be caused by the increase of tourism-related human activities. Meanwhile, FMF is as high as 0.8–0.9 during March and April and the lowest (~0.5) in summer.
3) *Central and eastern regions:* For the weakly absorbing type, both FMF and SSA at Nanjing and Hefei increase in summer, suggesting a joint increase of fine-mode particles and a decrease of aerosol absorption. At Shanghai and Zhoushan, SSA in summer and autumn are close and relatively low in winter and spring, while FMF is stable all year. For the mixed absorbing type, at Xi'an, SSA presents a clear dust feature in spring accompanying low FMF. At Beijing, the SSA is relatively low in spring together with smaller FMF, indicating absorption related to dust, while SSA is the lowest in winter with a small jump of FMF, suggesting absorbing fine particles. Overall, at these sites, SSA and FMF exhibit a mixed absorbing feature, that is, absorbing fine aerosols combined with dust particles.

Physical properties. Spatial variation. Figure 6 shows the multiyear average VPSD at SONET sites.

1) *Western and arid regions:* At Minqin, Zhangye, and Kashi, VPSD presents a large coarse mode that shows dominant mineral dust. At Lhasa, although the coarse mode is not comparable with other sites, it is still significantly higher than that of fine mode. The peak volumes of coarse-mode VPSD at these four sites are 0.07, 0.07, 0.20, and 0.03 $\mu m^3\ \mu m^{-2}$, respectively, but those of fine-mode VPSD are always less than 0.02 $\mu m^3\ \mu m^{-2}$.
2) *Tropical region:* At Sanya and Haikou, the coarse aerosol concentrations are relatively lower. The shapes of VPSD are similar to each other, with volume peak values of fine and coarse modes less than 0.05 and 0.03 $\mu m^3\ \mu m^{-2}$, respectively.
3) *Central and eastern regions:* VPSD shows significant fine mode at five densely populated sites (Guangzhou, Hefei, Shanghai, Nanjing, and Chengdu), with the maximum volume peak of fine mode up to 0.09 $\mu m^3\ \mu m^{-2}$ (Chengdu). At Harbin and Zhoushan, all fine- and coarse-mode VPSDs are not high (<0.05 $\mu m^3\ \mu m^{-2}$), suggesting relatively weak anthropogenic and natural aerosol sources. At Xi'an and Beijing, although VPSD embodies features of dust influence (i.e., considerable coarse mode), the larger fine mode (~0.05 $\mu m^3\ \mu m^{-2}$) illustrates a typical densely populated site feature.

Seasonal variations. The multiyear monthly average VPSD is shown in Fig. 7. For dust-dominated-type sites (Minqin, Zhangye, and Kashi), the coarse-mode volume is extremely high in spring while fine-mode volume is very low, and there is no significant change throughout the year (Xie et al. 2015; Xu et al. 2014). For tropical-type sites (Sanya and Haikou), both fine- and coarse-mode volumes are obviously low in summer, which might be caused by frequent scavenging and less emissions with decreased tourism activities during this season. For central and eastern sites (e.g., Hefei and Shanghai), the coarse-mode volume illustrates a decreasing trend in late summer related to monsoon scavenging, while both volume and peak radius of fine modes show a counterbalancing increase in roughly the same time window. This can be explained by the fact that impacts of hygroscopic

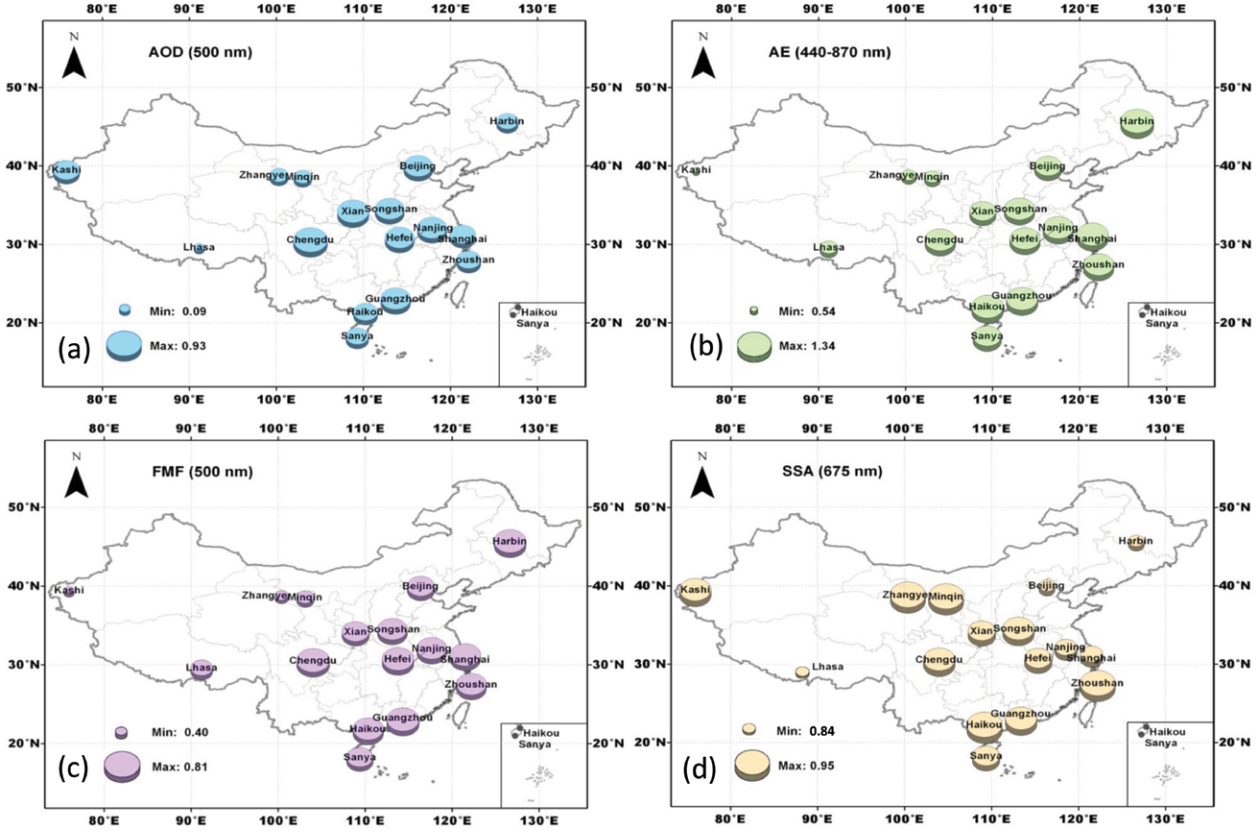

Fig. 3. Multiyear average (a) AOD (500 nm), (b) AE (440–870 nm), (c) FMF (500 nm), and (d) SSA (675 nm) at SONET sites.

growth are mainly related to fine-mode aerosols (Li et al. 2014). In addition, the volume of coarse mode increases clearly in spring at northern and central densely populated sites (e.g., Xi'an, Beijing, and Songshan).

Chemical properties. Spatial variation. The spatial distribution of five aerosol components is shown in Fig. 8. The BC and BrC mass concentrations at urban sites are generally higher than those at desert or coastal sites. For example, the sum of BC and BrC at Beijing (17 mg m^{-2}) is significantly higher than that at arid sites (e.g., only 1–2 mg m^{-2} at Kashi). The CM component (DU or SS) mainly from natural sources has evident spatial distribution variation. The CM concentrations at arid sites (e.g., Kashi, Minqin, and Zhangye) can exceed 600 mg m^{-2}, much larger than those at Chengdu, Nanjing, and Hefei, which are far from desert dust sources. The FS concentrations at large cities (e.g., Shanghai and Guangzhou) are basically higher than arid regions, and those at the coastal sites (e.g., Haikou) are also at a high level. AW content in aerosol is highly related to air humidity. The AW content at coastal sites can reach 120 mg m^{-2}, while that at arid regions is extremely low (3.5 mg m^{-2} at Lhasa).

Seasonal variations. Figure 9 shows the seasonal variations of aerosol component mass fractions and TMC at SONET sites. The average TMC of all sites is about 490 mg m^{-2} and shows very large site differences together with component fractions:

1) *Tropical and coastal regions*: Sanya, Haikou, and Guangzhou are mainly affected by maritime monsoon climate and have similar seasonal

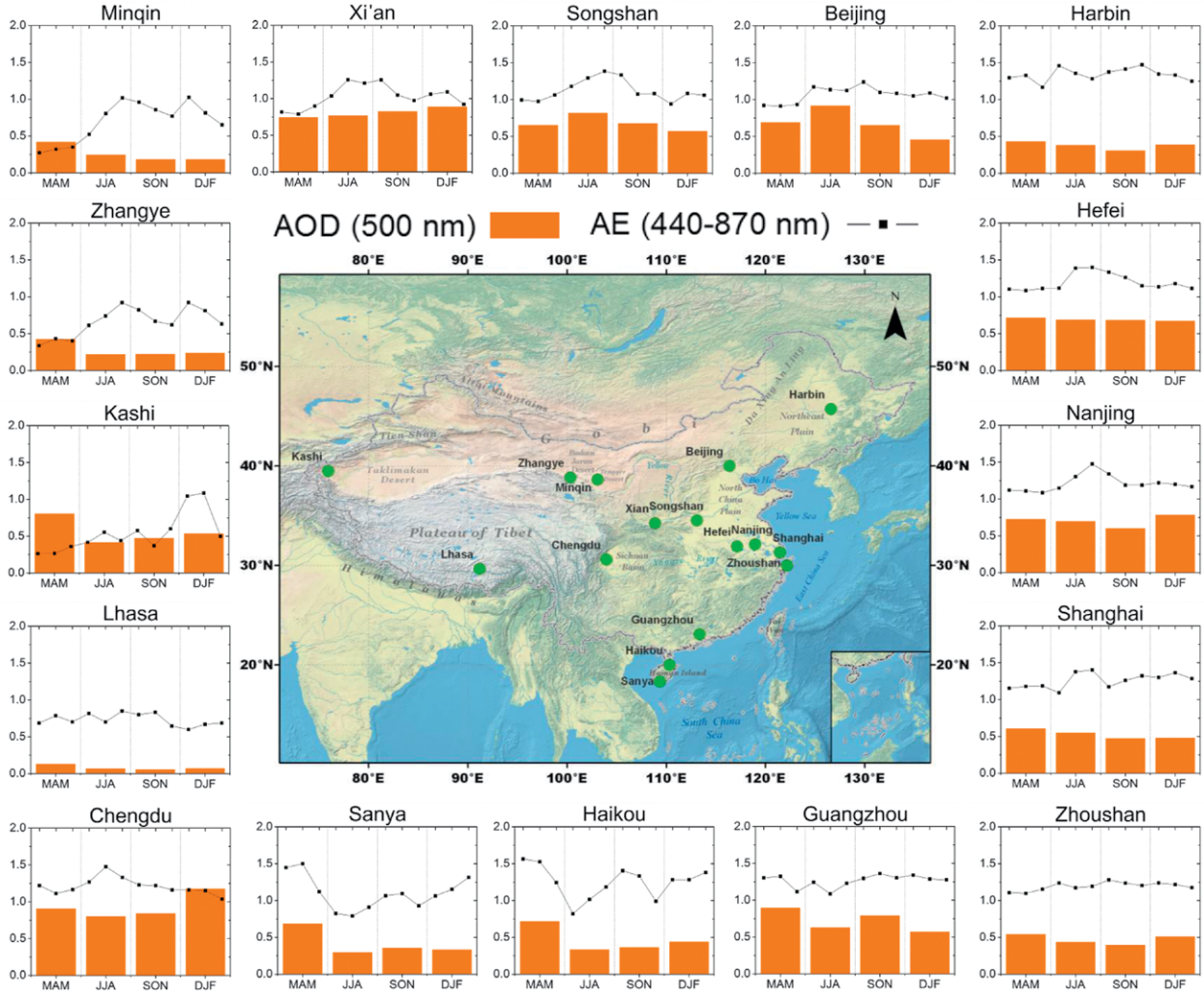

Fig. 4. Multiyear seasonal average AOD (500 nm) and monthly average AE (440–870 nm) at SONET sites. Seasons are spring [Mar–May (MAM)], summer [Jun–Aug (JJA)], autumn (Sep–Nov (SON)], and winter [Dec–Feb (DJF)].

characteristics. In spring, FS and CM (mainly SS) contribute up to 62% of TMC, and BC and BrC contents are relatively low. At Guangzhou, BC and BrC fractions are slightly higher in winter than other seasons, in accordance with Tao et al. (2014). Aerosol components at Zhoushan and Shanghai sites also show a similar seasonal pattern.

2) *Central and eastern regions*: The seasonal patterns at Hefei, Nanjing, and Chengdu are similar. The CM component is responsible for 54% of TMC in summer, lower than other seasons, while the strong atmospheric convection and frequent precipitation in summer result in an increase of AW components. The seasonal variations at Xi'an, Beijing, Songshan, and Harbin are comparable. In spring, the CM fractions generally exceed 60%–80% because of significant dust influences (Zhang et al. 2002; Liu et al. 2015). The anthropogenic components (e.g., FS, BC, and BrC) present an obvious increase in winter, due to additional emissions of coal combustion and atmosphere stagnation (Li et al. 2015).

3) *Western and arid regions*: Because of dry continental climate, aerosols at Minqin, Zhangye, and Kashi are similarly dominated (about 89%–96%) by CM components (mainly dust) throughout the year (Xu et al. 2014). There is no noticeable seasonal variation of components at Lhasa. CM dominates aerosol through the year, and TMC in spring (153 mg m^{-2}) is much higher than other seasons (only 95 mg m^{-2}).

Radiative properties. Atmospheric aerosols have direct influences on the Earth radiation budget through absorption and scattering of solar lights and further affect the energy balance of the Earth–atmospheric system accordingly (Sena et al. 2013). The aerosol direct RF is defined as the difference between the net flux with aerosol and that without aerosol (Babu et al. 2002; Adesina et al. 2014). The RFE (in units of W m^{-2} τ_{550}^{-1}) is defined as the rate at which the atmosphere is forced per unit of aerosol optical depth at 550 nm (García et al. 2011).

The daily average aerosol shortwave (0.3–2.8 μm) RF and RFE under clear-sky conditions is an important

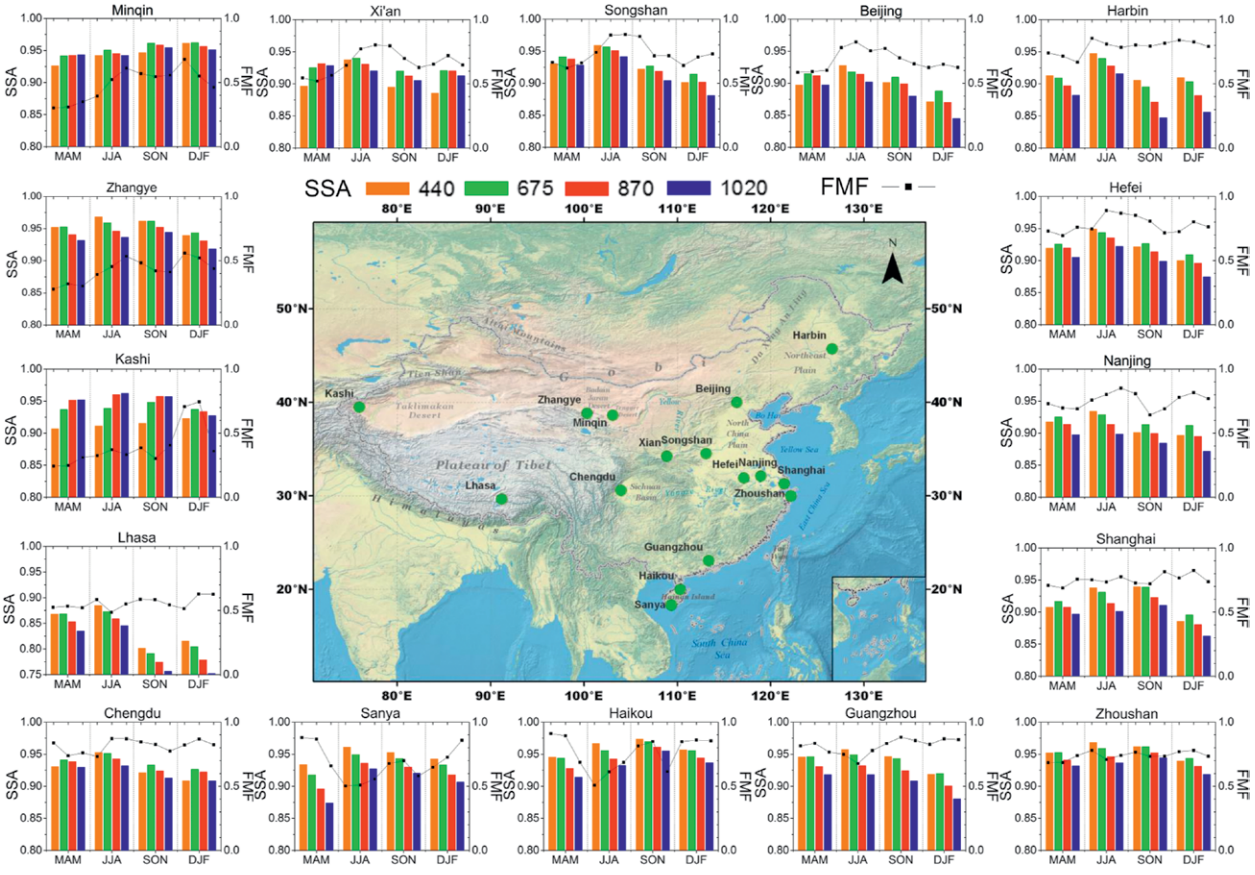

Fig. 5. Multiyear seasonal average spectral SSA (440, 675, 870, and 1,020 nm) and monthly average FMF (500 nm) at SONET sites. In each subfigure, the left and right *y* axes represent SSA and FMF, respectively. Bottom and top *x* axes are the seasons and months of the year.

reference for climate change assessment (García et al. 2011). The daily average aerosol parameters (AOD, SSA, *g*, and AE) at 440, 675, 870, and 1,020 nm and columnar water vapor content from SONET, as well as Moderate Resolution Imaging Spectroradiometer (MODIS) surface albedo product, are employed to calculate aerosol RF and RFE at SONET sites by using the Santa Barbara (Discrete Ordinate Radiative Transfer model) DISORT Atmospheric Radiative Transfer (SBDART) code. In the calculation, the daytime average aerosol products are used as alternatives of the daily average aerosol parameters.

From Fig. 10, it is clear that multiyear averages of daily average RF and RFE at all sites are negative, indicating radiative cooling effects, both at TOA and BOA.

1) *Tropical region*: RF_{BOA} at Sanya and Haikou are −30.25 and −30.64 W m^{-2}, respectively, with a very small difference. While at TOA, RF_{TOA} (−3.98 W m^{-2}) and RFE_{TOA} (−6.14 W m^{-2} τ_{550}^{-1}) at Sanya are lower (in absolute value) than those at Haikou, respectively.
2) *Western and arid regions*: RF and RFE at the Kashi, Zhangye, and Minqin sites are very close, both at TOA and BOA. The Lhasa site has the lowest radiative forcing effects among all sites, only −1.22 W m^{-2} (RF_{TOA}) and −1.39 W m^{-2} (RF_{BOA}).
3) *Central and eastern regions*: The anthropogenic aerosols have significant influences on the radiative parameters at these sites. The levels of RF clearly increase due to intensive human activities. At Beijing, the RF_{TOA} is −17.99 W m^{-2} and RF_{BOA} is −45.95 W m^{-2}, the highest values of all urban-type sites, but the RFE at the Beijing site is not the highest. In contrast, the RF_{TOA} and RFE_{TOA} at Shanghai are the lowest of all urban sites, but the RF_{BOA} and RFE_{BOA} are very high, suggesting strong cooling efficiency on the ground level. Overall, the RFE of densely populated region sites are systematically higher than other regions in China.

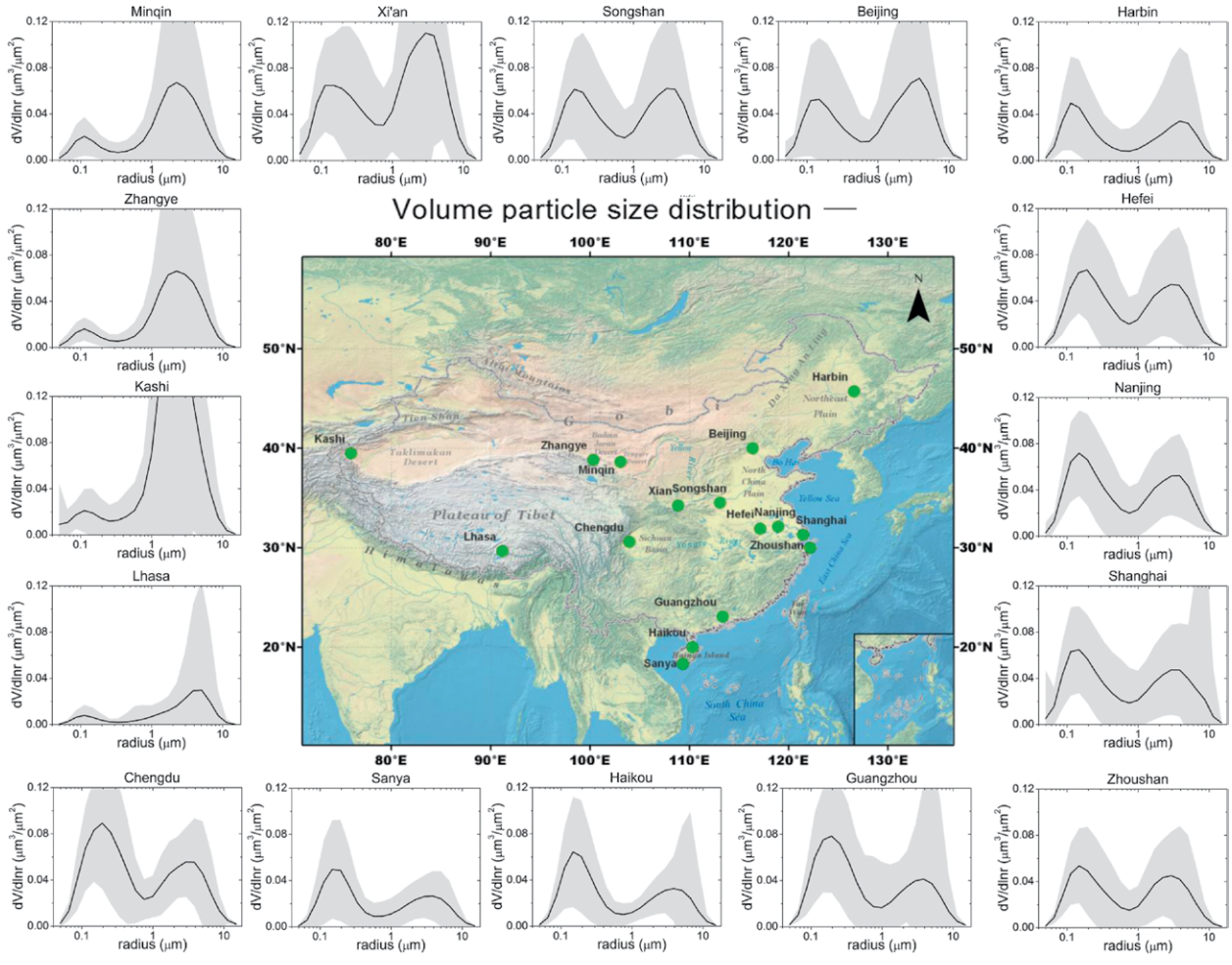

Fig. 6. The multiyear average VPSD at SONET sites. The gray shadings indicate standard deviations.

CONCLUSIONS. The SONET data are analyzed to carry out a comprehensive climatology study on total columnar aerosol properties over China. The results suggest that aerosols in China are complex and highly varied both in temporal and geographical scales. In the eastern region of China, the aerosol loading is high and anthropogenic influence is obvious, which accordingly results in significant radiative cooling effects both in top and bottom of the atmosphere. Major characteristics of total columnar aerosols at SONET sites include the following:

1) AOD is low in west China but high in east China. Lhasa is the cleanest site in SONET. AOD, together with AE and FMF, are rather high in the central and eastern zones. As for SSA, the strongest absorption occurs at Beijing, while the weakest absorption appears at Haikou. Because of dust impacts, the aerosol volume at western sites shows remarkable dominance of the coarse mode in spring, even all year. The highest fine-mode volume concentration occurs in Chengdu. As to temporal variations, AOD and AE at Lhasa and Zhoushan are stable in all seasons. In the tropical region (Sanya and Haikou), AOD, AE, and FMF are higher in spring, followed by a drop in summer when maritime aerosol is prevailing. In central and eastern China, FMF and SSA indicate plenty of fine particles and strong absorption, implying significant anthropogenic influences (e.g., winter heating, straw burning, and industrial emission).
2) The multiyear average TMC of all sites is about 490 mg m^{-2} with significant regional variations. The component fractions also show considerable spatial and seasonal variations. The western sites have the highest TMC consisting of a dominant dust component, while AW measurements are extremely low. In the tropical and coastal regions, aerosol TMC is relatively low and mainly

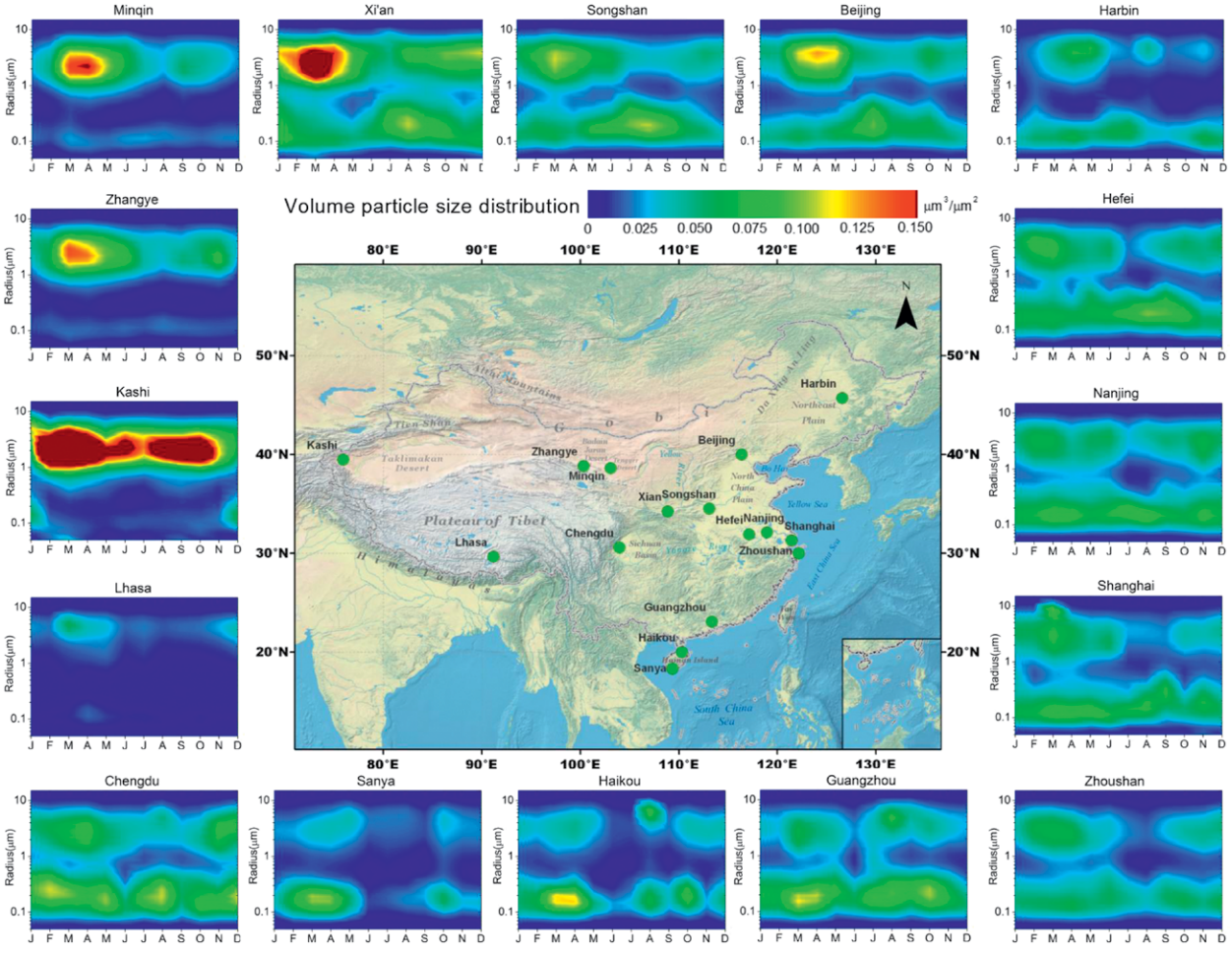

Fig. 7. The multiyear monthly average VPSD of SONET sites. The *x* axis is the month, and the *y* axis is the radius; color represents the volume concentration ($\mu m^3\ \mu m^{-2}$).

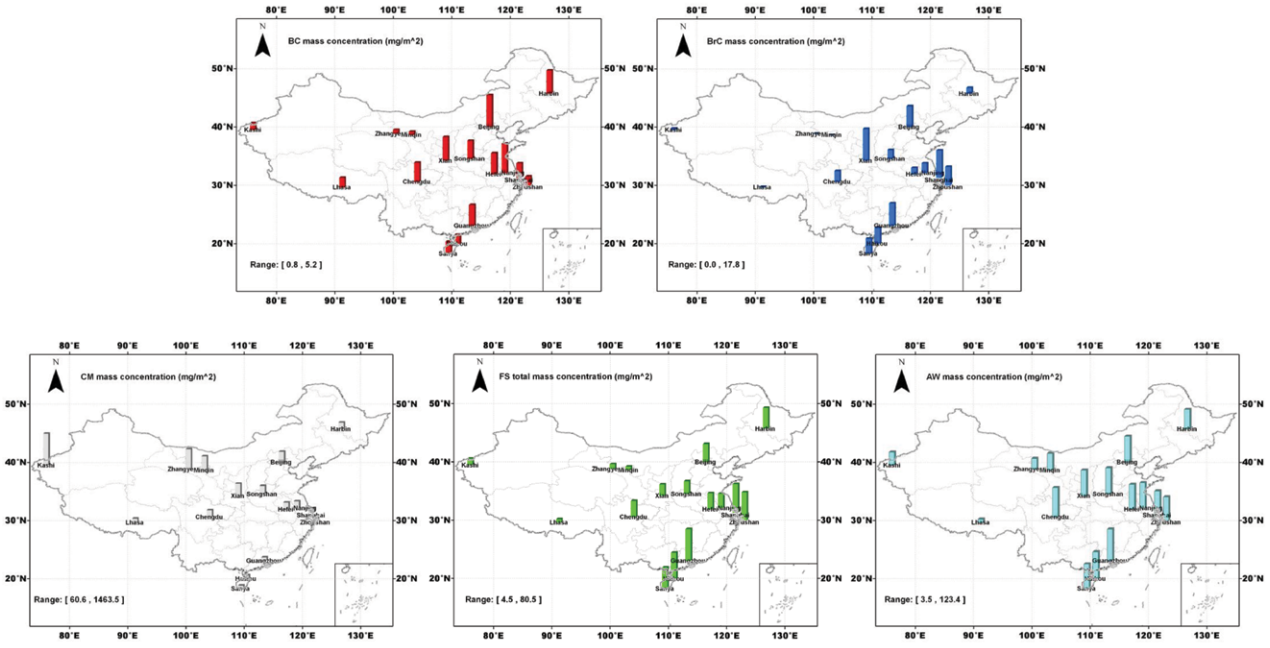

Fig. 8. The multiyear average mass concentration of aerosol components (BC, BrC, CM, FS, and AW) at SONET sites.

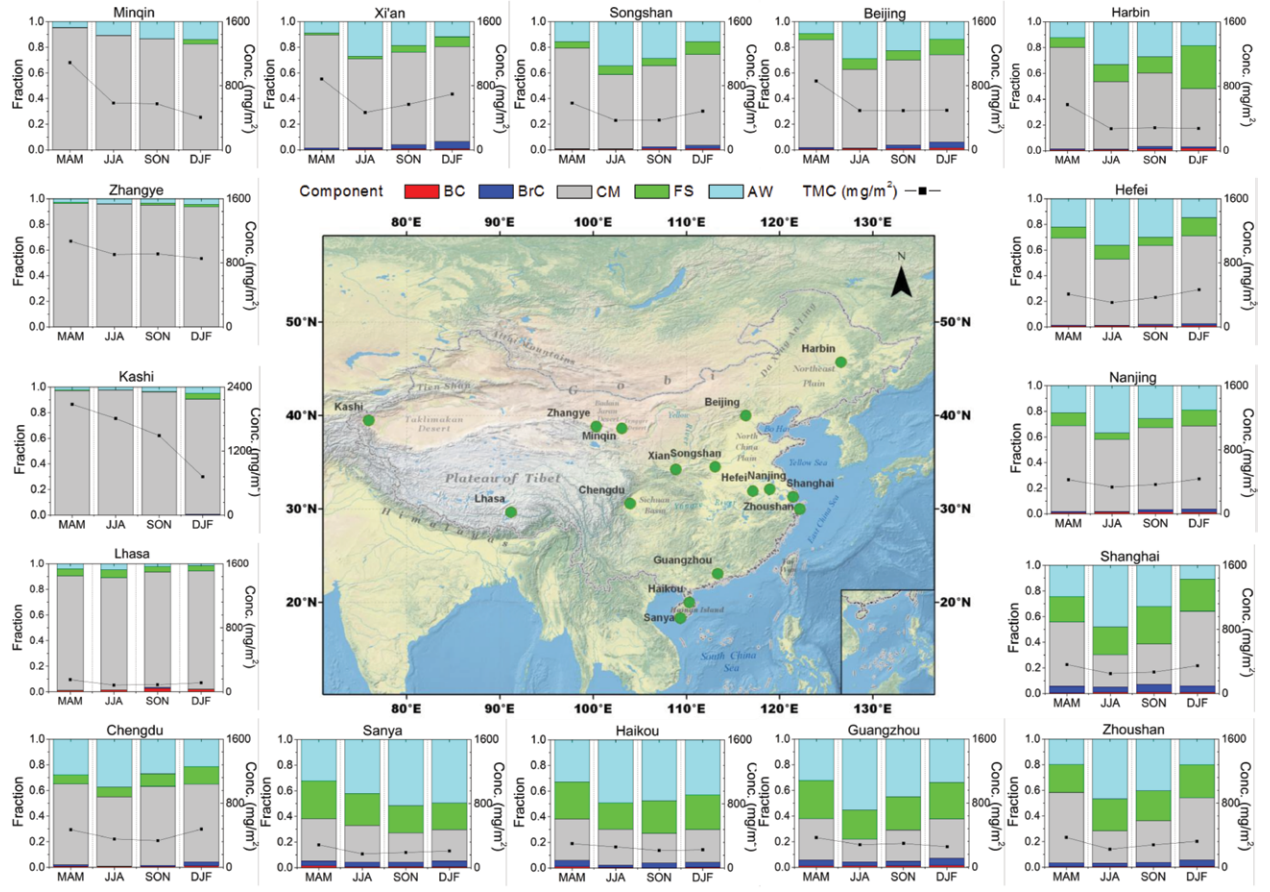

Fig. 9. Seasonal variations of aerosol component mass fractions and TMC at SONET sites.

composed of AW, SS, and FS. Aerosols in the central region present a transitional composition pattern, mostly featuring a significant dust contribution with varying AW fraction related to air humidity. Lhasa has the lowest TMC among all sites, with a majority of dust in mass. In terms of seasonal variation, most urban sites in central and eastern China show a generally higher level of carbonaceous components (sum of BC and BrC) in winter than in other seasons, most probably related to the increase of energy consumption in the heating season, especially coal burning.

3) Aerosol RF and RFE at all sites are negative both at TOA and BOA, indicating a climate cooling effect of China aerosols. The RF of densely populated region sites is larger than coastal region sites, and those of western and arid region sites are the smallest. The anthropogenic aerosol components have significant influences on RF and RFE in urban regions. The RF_{TOA} and RF_{BOA} at Beijing are the highest among all urban-type sites. The RFE_{BOA} at Shanghai is the highest among all urban-type sites. The RF_{TOA} and RF_{BOA} at Lhasa are the lowest among all sites.

For a long time, it was a big challenge to implement and maintain continuous comprehensive observation of total columnar atmospheric aerosols in China. SONET observation can contribute to deepening the understanding of aerosol properties over vast areas of China and improve knowledge of aerosols regarding climate change and air quality.

ACKNOWLEDGMENTS. This work is supported by National Key R&D Program of China (Grant 2016YFE0201400) and the National Natural Science Foundation of China (Grants 41671367 and 41671364). The authors wish to thank the AERONET team for its long-term support and are grateful to Philippe Goloub, Luc Blarel, and Thierry Podvin of PHOTONS for their help in data processing. The authors are grateful to Oleg Dubovik of University Lille 1, France, for providing aerosol inversion help. We thank Cimel Electronique, Paris, France, for support on the sun–sky radiometers. We also thank Xiaobing Zheng and Jianjun Li from the Anhui Institute of Optics and Fine Mechanics, Chinese Academy of Sciences, for helping with calibration of the radiometers.

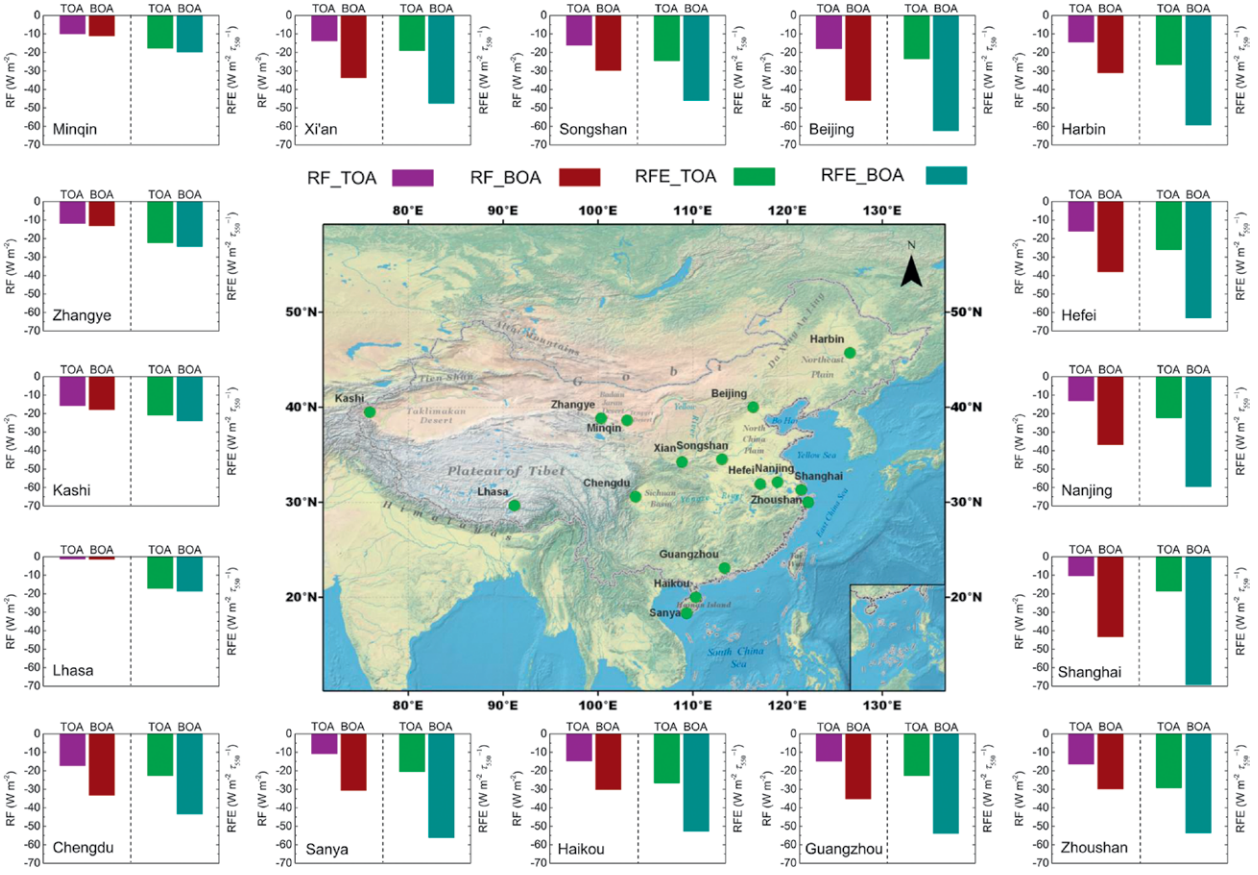

Fig. 10. The multiyear average of daily average shortwave aerosol RF and RFE (left and right parts, respectively, in each graph) at SONET sites.

REFERENCES

Adesina, A. J., K. R. Kumar, V. Sivakumar, and D. Griffith, 2014: Direct radiative forcing of urban aerosols over Pretoria (25.75°S, 28.28°E) using AERONET Sunphotometer data: First scientific results and environmental impact. *J. Environ. Sci.*, **26**, 2459–2474, https://doi.org/10.1016/j.jes.2014.04.006.

Babu, S. S., S. K. Satheesh, and K. K. Moorthy, 2002: Aerosol radiative forcing due to enhanced black carbon at an urban site in India. *Geophys. Res. Lett.*, **29**, 1880, https://doi.org/10.1029/2002GL015826.

Che, H. Z., and Coauthors, 2009: Instrument calibration and aerosol optical depth validation of the China Aerosol Remote Sensing Network. *J. Geophys. Res.*, **114**, D03206, https://doi.org/10.1029/2008JD011030.

Dubovik, O., and M. D. King, 2000: A flexible inversion algorithm for retrieval of aerosol optical properties from Sun and sky radiance measurements. *J. Geophys. Res.*, **105**, 20 673–20 696, https://doi.org/10.1029/2000JD900282.

——, A. Smirnov, B. N. Holben, M. D. King, Y. J. Kaufman, T. F. Eck, and I. Slutsker, 2000: Accuracy assessments of aerosol optical properties retrieved from Aerosol Robotic Network (AERONET) Sun and sky radiance measurements. *J. Geophys. Res.*, **105**, 9791–9806, https://doi.org/10.1029/2000JD900040.

——, B. Holben, T. F. Eck, A. Smirnov, Y. J. Kaufman, M. D. King, D. Tanré, and I. Slutsker, 2002: Variability of absorption and optical properties of key aerosol types observed in worldwide locations. *J. Atmos. Sci.*, **59**, 590–608, https://doi.org/10.1175/1520-0469(2002)059<0590:VOAAOP>2.0.CO;2.

——, and Coauthors, 2006: Application of spheroid models to account for aerosol particle nonsphericity in remote sensing of desert dust. *J. Geophys. Res.*, **111**, D11208, https://doi.org/10.1029/2005JD006619.

Eck, T. F., and Coauthors, 2010: Climatological aspects of the optical properties of fine/coarse mode aerosol mixtures. *J. Geophys. Res.*, **115**, D19205, https://doi.org/10.1029/2010JD014002.

Ganguly, D., P. Ginoux, V. Ramaswamy, O. Dubovik, J. Welton, E. A. Reid, and B. N. Holben, 2009: Inferring the composition and concentration of aerosols by combining AERONET and MPLNET data: Comparison with other measurements and utilization to evaluate GCM output. *J. Geophys. Res.*, **114**, D16203, https://doi.org/10.1029/2009JD011895.

García, O. E., F. J. Expósito, J. P. Díaz, and A. M. Díaz, 2011: Radiative forcing under mixed aerosol conditions. *J. Geophys. Res.*, **116**, D01201, https://doi.org/10.1029/2009JD013625.

Holben, B. N., and Coauthors, 1998: AERONET—A federated instrument network and data archive for aerosol characterization. *Remote Sens. Environ.*, **66**, 1–16, https://doi.org/10.1016/S0034-4257(98)00031-5.

——, T. F. Eck, I. Slutsker, A. Smirnov, A. Sinyuk, J. Schafer, D. Giles, and O. Dubovik, 2006: Aeronet's version 2.0 quality assurance criteria. *Remote Sensing of the Atmosphere and Clouds*, S.-C. Tsay et al., Eds., Society of Photo-Optical Instrumentation Engineers (SPIE Proceedings, Vol. 6408), 64080Q, https://doi.org/10.1117/12.706524.

——, and Coauthors, 2018: An overview of mesoscale aerosol processes, comparisons, and validation studies from DRAGON networks. *Atmos. Chem. Phys.*, **18**, 655–671, https://doi.org/10.5194/acp-18-655-2018.

Hu, Y., 1935: The distribution of population in China, with statistics and maps. *Acta Geogr. Sin.*, **2**, 33–74.

Huang, X., P. Yang, G. Kattawar, and K. N. Liou, 2015: Effect of mineral dust aerosol aspect ratio on polarized reflectance. *J. Quant. Spectrosc. Radiat. Transfer*, **151**, 97–109, https://doi.org/10.1016/j.jqsrt.2014.09.014.

IPCC, 2013: *Climate Change 2013: The Physical Science Basis*. Cambridge University Press, 1535 pp., https://doi.org/10.1017/CBO9781107415324.

Kim, D.-H., B.-J. Sohn, T. Nakajima, T. Takamura, T. Takemura, B.-C. Choi, and S.-C. Yoon, 2004: Aerosol optical properties over east Asia determined from ground-based sky radiation measurements. *J. Geophys. Res.*, **109**, D02209, https://doi.org/10.1029/2003JD003387.

Li, Z., P. Goloub, L. Blarel, B. Damiri, T. Podvin, and I. Jankowiak, 2007: Dust optical properties retrieved from ground-based polarimetric measurements. *Appl. Opt.*, **46**, 1548–1553, https://doi.org/10.1364/AO.46.001548.

——, L. Blarel, T. Podvin, P. Goloub, J.-P. Buis, and J.-P. Morel, 2008: Transferring the calibration of direct solar irradiance to diffuse-sky radiance measurements for CIMEL Sun-sky radiometers. *Appl. Opt.*, **47**, 1368–1377, https://doi.org/10.1364/AO.47.001368.

——, and Coauthors, 2013: Aerosol physical and chemical properties retrieved from ground-based remote sensing measurements during heavy haze days in Beijing winter. *Atmos. Chem. Phys.*, **13**, 10 171–10 183, https://doi.org/10.5194/acp-13-10171-2013.

——, and Coauthors, 2014: Aerosol physical, chemical and optical properties observed in the ambient atmosphere during haze pollution conditions. *40th COSPAR Scientific Assembly*, Moscow, Russia, Lomonosov Moscow State University, Abstract A1.1-57-14.

——, L. Li, F. Zhang, D. Li, Y. Xie, and H. Xu, 2015: Comparison of aerosol properties over Beijing and Kanpur: Optical, physical properties and aerosol component composition retrieved from 12 years ground-based Sun-sky radiometer remote sensing data. *J. Geophys. Res. Atmos.*, **120**, 1520–1535, https://doi.org/10.1002/2014JD022593.

——, and Coauthors, 2018: Calibration of the degree of linear polarization measurements of the polarized Sun-sky radiometer based on the POLBOX system. *Appl. Opt.*, **57**, 1011–1018, https://doi.org/10.1364/AO.57.001011.

Liu, Z., B. Hu, L. Wang, F. Wu, W. Gao, and Y. Wang, 2015: Seasonal and diurnal variation in particulate matter (PM_{10} and $PM_{2.5}$) at an urban site of Beijing: Analyses from a 9-year study. *Environ. Sci. Pollut. Res.*, **22**, 627, https://doi.org/10.1007/s11356-014-3347-0.

Nakajima, T., and Coauthors, 2007: Overview of the Atmospheric Brown Cloud East Asian Regional Experiment 2005 and a study of the aerosol direct radiative forcing in east Asia. *J. Geophys. Res.*, **112**, D24S91, https://doi.org/10.1029/2007JD009009.

O'Neill, N. T., O. Dubovik, and T. F. Eck, 2001: Modified Ångström exponent for the characterization of submicrometer aerosols. *Appl. Opt.*, **40**, 2368–2375, https://doi.org/10.1364/AO.40.002368.

Peel, M. C., B. L. Finlayson, and T. A. McMahon, 2007: Updated world map of the Köppen–Geiger climate classification. *Hydrol. Earth Syst. Sci.*, **11**, 1633–1644, https://doi.org/10.5194/hess-11-1633-2007.

Rosenfeld, D., Y. Rudich, and R. Lahav, 2001: Desert dust suppressing precipitation: A possible desertification feedback loop. *Proc. Natl. Acad. Sci. USA*, **98**, 5975–5980, https://doi.org/10.1073/pnas.101122798.

Schuster, G. L., O. Dubovik, B. N. Holben, and E. E. Clothiaux, 2005: Inferring black carbon content and specific absorption from Aerosol Robotic Network (AERONET) aerosol retrievals. *J. Geophys. Res.*, **110**, D10S17, https://doi.org/10.1029/2004JD004548.

Sena, E. T., P. Artaxo, and A. L. Correia, 2013: Spatial variability of the direct radiative forcing of biomass burning aerosols and the effects of land use change in Amazonia. *Atmos. Chem. Phys.*, **13**, 1261–1275, https://doi.org/10.5194/acp-13-1261-2013.

Tao, J., and Coauthors, 2014: Impact of $PM_{2.5}$ chemical compositions on aerosol light scattering in Guangzhou—The largest megacity in South China. *Atmos. Res.*, **135–136**, 48–58, https://doi.org/10.1016/j.atmosres.2013.08.015.

Wang, L., and Coauthors, 2013: Estimate of aerosol absorbing components of black carbon, brown carbon, and dust from ground-based remote sensing data of sun-sky radiometers. *J. Geophys. Res. Atmos.*, **118**, 6534–6543, https://doi.org/10.1002/jgrd.50356.

Xie, Y., Z. Li, D. Li, H. Xu, and K. Li, 2015: Aerosol optical and microphysical properties of four typical sites of SONET in China based on remote sensing measurements. *Remote Sens.*, **7**, 9928–9953, https://doi.org/10.3390/rs70809928.

Xin, J., and Coauthors, 2007: Aerosol optical depth (AOD) and Ångström exponent of aerosols observed by the Chinese Sun Hazemeter Network from August 2004 to September 2005. *J. Geophys. Res.*, **112**, D05203, https://doi.org/10.1029/2006JD007075.

Xu, H., and Coauthors, 2014: Ground-based polarimetric remote sensing of dust aerosol properties in Chinese deserts near Hexi Corridor. *Adv. Meteor.*, **2014**, 240452, https://doi.org/10.1155/2014/240452.

Zhang, X. Y., J. J. Cao, L. M. Li, R. Arimoto, Y. Cheng, B. Huebert, and D. Wang, 2002: Characterization of atmospheric aerosol over XiAn in the South Margin of the Loess Plateau, China. *Atmos. Environ.*, **36**, 4189–4199, https://doi.org/10.1016/S1352-2310(02)00347-3.

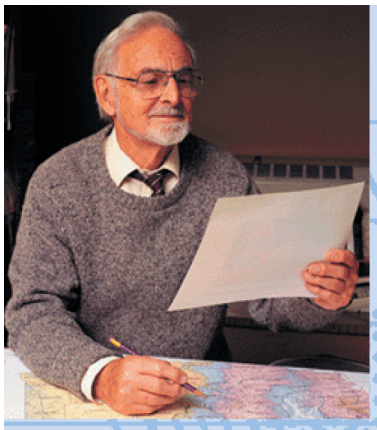

A Half Century of Progress in Meteorology: A Tribute to Richard Reed

edited by Richard H. Johnson and Robert A. Houze Jr.

with selections by: Lance F. Bosart Robert W. Burpee Anthony Hollingsworth James R. Holton Brian J. Hoskins Richard S. Lindzen John S. Perry Erik A. Rasmussen Adrian Simmons Pedro Viterbo

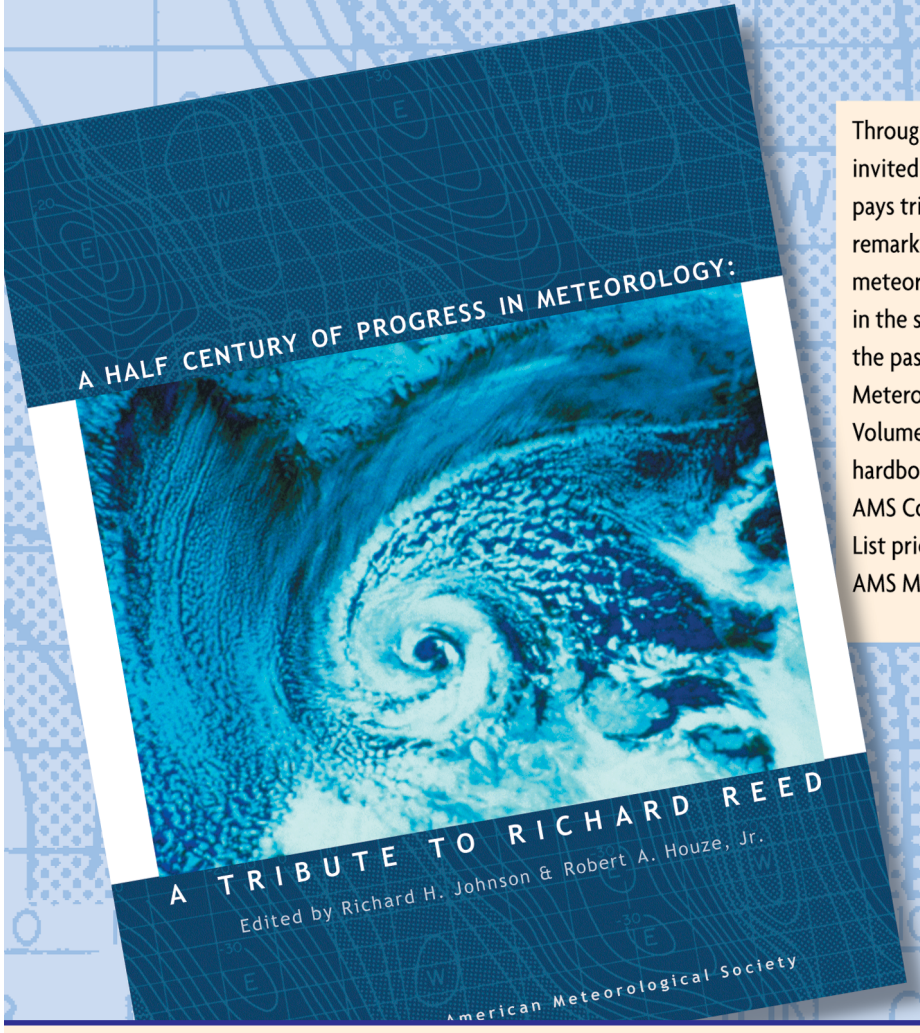

Through a series of reviews by invited experts, this monograph pays tribute to Richard Reed's remarkable contributions to meteorology and his leadership in the science community over the past 50 years. 2003. Meterological Monograph Series, Volume 31, Number 53; 139 pages, hardbound; ISBN 1-878220-58-6; AMS Code MM53.
List price: $80.00
AMS Member price: $60.00

Order Online from bookstore.ametsoc.org